



Dynamic metabolic and molecular changes during seasonal shrinking in *Sorex araneus*

William R. Thomas, Cecilia Baldoni, Yuanyuan Zeng, et al.

Genome Res. published online November 4, 2025

Access the most recent version at doi:[10.1101/gr.280639.125](https://doi.org/10.1101/gr.280639.125)

P<P	Published online November 4, 2025 in advance of the print journal.
Accepted Manuscript	Peer-reviewed and accepted for publication but not copyedited or typeset; accepted manuscript is likely to differ from the final, published version.
Open Access	Freely available online through the <i>Genome Research</i> Open Access option.
Creative Commons License	This manuscript is Open Access. This article, published in <i>Genome Research</i> , is available under a Creative Commons License (Attribution-NonCommercial 4.0 International license), as described at http://creativecommons.org/licenses/by-nc/4.0/ .
Email Alerting Service	Receive free email alerts when new articles cite this article - sign up in the box at the top right corner of the article or click here .



To subscribe to *Genome Research* go to:
<https://genome.cshlp.org/subscriptions>

Published by Cold Spring Harbor Laboratory Press

1 Title: Dynamic metabolic and molecular changes during seasonal shrinking in *Sorex araneus*

2
3 Running title: Seasonal metabolic and molecular changes in *Sorex araneus*

4
5
6 William R. Thomas^{1*}, Cecilia Baldoni^{2,3}, Yuanyuan Zeng⁴, David Carlson¹, Julie Holm-
7 Jacobsen⁴, Marion Muturi², Dominik von Elverfeldt⁵, Tue B. Bennike, Dina K. N. Dechmann^{2,3},
8 John Nieland⁴, Angelique P. Corthals^{6¶}, Liliana M. Dávalos^{1,7¶} *

9
10
11 ¹Department of Ecology and Evolution, Stony Brook University; Stony Brook, NY 11794,
12 United States.

13
14 ²Max-Planck Institute of Animal Behavior; Radolfzell, 78315, Germany.

15
16 ³University of Konstanz; Konstanz, 78464, Germany.

17
18 ⁴Health Science and Technology, Aalborg University; Gistrup, 9260, Denmark.

19
20 ⁵Division of Medical Physics, Department of Diagnostic and Interventional Radiology,
21 University Medical Center Freiburg, Faculty of Medicine, University of Freiburg, Freiburg,
22 79106, Germany.

23
24 ⁶John Jay College of Criminal Justice; New York, NY 10019, United States.

25
26 ⁷Consortium for Inter-Disciplinary Environmental Research, Stony Brook University; Stony
27 Brook, NY 11794, United States.

28
29 * Corresponding authors: William R. Thomas and Liliana M. Dávalos

30 **Emails:** William.thomas@stonybrook.edu, Liliana.Davalos@stonybrook.edu

31
32
33
34 [¶] These authors contributed equally to this work.

35 **Abstract**

36 To meet the challenge of wintering in place, many high-latitude small mammals reduce energy
37 demands through hibernation. In contrast, short-lived Eurasian common shrews, *Sorex araneus*,
38 remain active and shrink, including energy-intensive organs in winter, regrowing in spring in an
39 evolved strategy called Dehnel's phenomenon. How this size change is linked to metabolic and
40 regulatory changes to sustain their high metabolism is unknown. We analyzed metabolic,
41 proteomic, and gene expression profiles spanning the entirety of Dehnel's seasonal cycle in wild
42 shrews. We show regulatory changes to oxidative phosphorylation and increased fatty acid
43 metabolism during autumn-to-winter shrinkage, as previously found in hibernating species. But in
44 shrews we also found upregulated winter expression of genes involved in gluconeogenesis: the
45 biosynthesis of glucose from non-carbohydrate substrates. Co-expression models revealed
46 changes in size and metabolic gene expression interconnect via FOXO signaling, whose
47 overexpression reduces size and extends lifespan in many model organisms. We propose that
48 while shifts in gluconeogenesis meet the challenge posed by high metabolic rate and active winter
49 lifestyle, FOXO signaling is central to Dehnel's phenomenon, with spring downregulation
50 limiting lifespan in these shrews.

51

52 **Introduction**

53 Wintering adaptations vary widely across animals and the most common strategies are conserving
54 energy by lowering metabolic rates and activity (e.g., hibernation or torpor) and migration. By
55 contrast, a handful of species that neither migrate nor slow their metabolism have evolved a
56 different wintering size plasticity known as Dehnel's phenomenon (Dehnel 1949; Pucek 1965b;
57 Lázaro et al. 2018; Lázaro and Dechmann 2021). This pattern of growth, best studied in the
58 Eurasian common shrew, *Sorex araneus*, is unlike that of almost every other mammal. Instead of
59 growing continuously to adulthood, juvenile *S. araneus* grow to an initial maximum size in the

60 first summer of their disproportionately brief life (~1 year). In anticipation of harsh winter
61 conditions, shrews then shrink, reaching a nadir in winter, followed by rapid regrowth to their
62 adult, breeding size in spring. This plasticity is not just a retooling of overall body size, but also
63 occurs in many vital organs, including the liver, brain, and spleen (Pucek 1965a, 1965b).
64 Although Dehnel's phenomenon has garnered much interest because of its potential for
65 regenerating organs (Ray et al. 2020), metabolic and regulatory changes during this wintering
66 adaptation remain largely unknown.

67

68 Dehnel's phenomenon corresponds to the unique physiological constraints shrews face. *S.*
69 *araneus* have one of the highest mammalian metabolic rates measured to date (Genoud et al.
70 2018), requiring high and constant food intake throughout the year (Keicher et al. 2017). But
71 supplying energy to maintain this high metabolic rate is especially difficult in autumn and winter,
72 when temperatures decrease and resources become scarce (Churchfield et al. 2012; Hyvärinen
73 1984). Therefore, Dehnel's phenomenon is construed as an evolutionary adaptation that
74 compensates for continuously high energetic demands by reducing body and organ size,
75 particularly of energy-expensive tissue (Lázaro et al. 2019). In support of this hypothesis,
76 absolute resting metabolic rate decreases with shrew size in winter, while mass-specific rate
77 remains the same (Hyvärinen 1984; Taylor et al. 2013; Schaeffer et al. 2020)

78

79 Wintering strategies encompass a spectrum of related traits and physiological processes (Auteri
80 2022). Changes in other wintering strategies, such as metabolic shifts observed in hibernation
81 (Boyer and Barnes 1999; Chazarin et al. 2019; Weir et al. 2024), may thus share common
82 mechanisms with those involved in Dehnel's phenomenon. For example, mechanistic analyses of
83 mammalian hibernation have identified a toolkit of genes that regulates vast metabolic changes
84 (Boyer and Barnes 1999; Chazarin et al. 2019; Faherty et al. 2016), including those associated

85 with increased fatty acid oxidation (Villanueva-Cañas et al. 2014), as hibernators rely on gradual
86 fat utilization over winter. Research on shrew physiology indicates they also rely extensively on
87 lipid metabolism in winter (Keicher et al. 2017) and may share some molecular mechanisms with
88 hibernation.

89

90 But *S. araneus* remain active throughout winter, undergoing drastic shrinkage while navigating a
91 metabolically demanding environment. This active wintering strategy contrasts with hibernation,
92 suggesting key differences in metabolic and regulatory processes. For example, wintering shrews
93 show rapid fat turnover, with 50% fat turnover rates decreasing from 4.5 hours in summer
94 juveniles to 2.5 hours in winter (Keicher et al. 2017). Consequently, metabolic profiles may differ
95 significantly between these strategies. In hibernators there is also a downregulation of genes
96 involved in glucose breakdown (Villanueva-Cañas et al. 2014). In general, when energy stores are
97 depleted, glucose is produced in the liver through gluconeogenesis. This glucose is then released
98 into the bloodstream and metabolized in the mitochondria via oxidative phosphorylation (Rui
99 2014). Unlike hibernators that suppress this response, wintering shrews seem to increase this
100 starvation response as environments become harsher (Hyvärinen 1984). Thus, we hypothesized
101 that shrews shrink by upregulating fatty acid metabolism, with potential similarities to hibernators
102 though, unlike hibernators, shrews supplement their energy budget with glucose to maintain their
103 active winter lifestyle.

104

105 To examine metabolic dynamics and regulatory changes throughout Dehnel's phenomenon, and
106 its potential parallels to other wintering strategies, we conducted a multi-omic analysis of *S.*
107 *araneus* across seasonal timepoints that match the trajectory of size plasticity. We focused on
108 blood, which circulates metabolites, and the liver, a key site of metabolic regulation including
109 lipid and glucose processing. By integrating phenotypic, metabolomic, transcriptomic, and

110 proteomic data, our study aims to identify the molecular pathways that orchestrate seasonal
111 changes in body size, and to explore how these pathways may be linked to metabolism and
112 longevity in small, actively wintering mammals.

113

114 **Results**

115 *Dehnel's phenomenon in German shrew population*

116 Comparisons of body mass throughout the cycle confirmed patterns of size changes (Fig. 1A).
117 Analyzing the 24 shrews collected for all stages of Dehnel's phenomenon (Supplemental Data S1
118 and Supplemental Table S1: large summer juvenile n=5; shrinking autumn juvenile n=4; small
119 winter juvenile n=5; regrowing spring adult n=5; regrown Summer Adult n=5), we found (*t*-test)
120 body mass shrank as expected between summer juveniles and winter juveniles (body mass=-1.00
121 g, $p=0.03$) with regrowth as they matured to spring adults (body mass=+3.72 g, $p<0.0001$)
122 (Supplemental Table S2). Shrew liver mass reached a minimum as autumn juveniles (liver
123 mass=-0.09 g, $p=0.09$) (Supplemental Table S3), with the significant portion of regrowth
124 occurring between the winter juvenile and spring adult phases (liver mass=+0.54 g, $p<0.001$).
125 These size changes both validated previous research and were used to guide metabolomic,
126 transcriptomic, and proteomics characterization of Dehnel's phenomenon.

127

128 *Metabolomic shifts in lipid metabolite concentrations*

129 We characterized the blood plasma metabolome (Supplemental Data S2) to quantify metabolites
130 throughout the cycle and evaluated the potential shifts in metabolism during shrinkage and
131 regrowth. We validated 250 metabolites found in all seasons with multiple detection methods
132 (Supplemental Data S3). Normalized concentrations of these metabolites clustered according to
133 season (Supplemental Fig. S1A/B). We found 28 with significant differences in mean
134 concentration across the stages of Dehnel's phenomenon ($p<0.05$) (Fig. 1B/Supplemental Table

135 S4/Supplemental Fig. S1C). Among differentially concentrated metabolites, three were lipid
136 metabolites; arachidonic acid (AA, $p=0.04$, $F=5.78$), ethyl palmitoleate (EP, $p=0.02$, $F=6.79$), and
137 docosahexanoic acid (DHA, $p=0.04$, $F=5.86$). These three lipid metabolites showed significant
138 decreases in peak area, a proxy for concentration, between summer juveniles and other stages of
139 size change (autumn juveniles, winter juveniles, spring adults), especially in winter juveniles
140 (AA= -8.7×10^7 peak area, DHA= -1.2×10^8 peak area, EP= -3.1×10^6 peak area), for which the
141 concentrations of DHA and AA were at their minimum.

142

143 ***Global liver gene expression patterns reflect seasonal body size plasticity***

144 To understand how gene expression in the liver changes across seasonal stages – and whether
145 these shifts align with the body size changes of Dehnel’s phenomenon – we began by examining
146 the global transcriptomic patterns (Supplemental Data S4). Exploratory analyses of liver gene
147 expression revealed patterns that mirror seasonal changes in body size. Using a likelihood ratio
148 test (LRT), we compared the full model (\sim sex+season) to a null model with only an intercept
149 (\sim 1). This test identified 3336 genes whose expression was significantly associated with seasonal
150 stage ($p_{\text{adj}} < 0.01$, Supplemental Data S4). Principal component analysis (PCA) of these significant
151 genes showed clear seasonal clustering, with PC1 and PC2 explaining 22.3% and 13.4% of the
152 variation, respectively (Supplemental Fig. S2A). Hierarchical clustering supports this structure,
153 grouping samples into three major clusters: one composed of summer juveniles, another including
154 shrinking autumn and winter juveniles, and a third encompassing spring and summer adults
155 (Supplemental Fig. S2B).

156

157 To investigate the temporal dynamics of gene regulation, we further clustered the 3,336
158 significant genes based on their expression patterns across seasons (Fig. 2B and Supplemental

159 Fig. S2C). This analysis distinguished four gene expression clusters with greater than 150 genes
160 (Supplemental Data S4). Clusters 1 (n=580 genes) and 2 (n=156 genes) displayed consistent
161 increases or decrease in expression across timepoints, suggesting that they are more reflective of
162 ontogeny than of seasonal plasticity. In contrast, Clusters 3 (n=312 genes) and 4 (n=887 genes)
163 exhibited expression changes consistent with Dehnel's phenomenon. Specifically, Cluster 3 genes
164 were downregulated during shrinkage (autumn and winter) and strongly upregulated during
165 regrowth. Conversely, Cluster 4 genes showed the opposite pattern – upregulated during
166 shrinkage and downregulated as body size increased. Between Clusters 3 and 4, only two
167 pathways were significantly enriched: protein processing in the endoplasmic reticulum
168 ($p_{\text{adj}} < 0.0001$) and proteasome ($p_{\text{adj}} < 0.05$) (Supplemental Data S4 and Supplemental Table S5).

169

170 *Transcriptomic signatures of winter shrinkage*

171 Results showed many differentially expressed genes in the liver between summer juveniles and
172 winter juveniles (shrinking stage), with an upregulation of genes related to mitochondrial, lipid,
173 and glucose metabolism (Supplemental Data S5). Comparisons revealed 964 differentially
174 expressed genes ($p_{\text{adj}} < 0.05$), with 497 significantly upregulated and 467 significantly
175 downregulated in winter juveniles (Fig. 3A). We then used a ranked gene set enrichment test to
176 identify functional effects of RNA regulatory change. This analysis identified 25 pathways
177 enriched with differentially expressed genes (21 upregulated and 4 downregulated) (Fig. 4A,
178 Supplemental Data S5). Oxidative phosphorylation was the most enriched pathway ($p_{\text{adj}} < 0.001$,
179 Normalized Enrichment Score=2.34, [NES]) consisting of 46 genes. This gene set included 21
180 upregulated genes that encode mitochondrial complex I subunit proteins (NDUFs) and 19
181 upregulated genes encoding ATPases and synthases (Supplemental Fig. S3), suggesting pathway
182 activation. Other important pathways, based on initial hypotheses from previous Dehnel's
183 research described in the introduction, enriched with upregulated genes included glycolysis and

184 gluconeogenesis ($p_{\text{adj}} < 0.001$, NES=2.09) (Supplemental Fig. S4), which contained the gene
185 encoding for glucose-6 phosphatase catalytic subunit 1, *G6PCI* ($p_{\text{adj}} = 0.41$, Log Fold
186 Change=0.30, [LFC]) (Fig. 4B), and fatty acid metabolism ($p_{\text{adj}} < 0.01$, NES=1.81) (Supplemental
187 Fig. S5).

188

189 *Proteomic validation of metabolic pathway shifts*

190 We validated changes in metabolism-related gene expression between summer juveniles and
191 winter juveniles (shrinking stage) with liver proteomics (Supplemental Data S6). Despite the liver
192 proteomics (n=1,377 proteins) data set being smaller than the gene expression set (n=24,205
193 transcripts), there was substantial overlap in direction, significance, and pathway enrichment of
194 changes between the two (Supplemental Fig. 6, Fig. S3). Using a linear model to estimate the
195 correlation between differential change (summer juveniles vs winter juveniles) in gene expression
196 and protein abundance, we found that LFC in gene expression was significantly associated with
197 LFC in protein abundance ($F = 197.5$, $df = 1373$, $p < 0.001$), but the model only explains a fraction of
198 the variation between them ($R^2 = 0.13$) (Fig. 3A). However, this correlation is congruent with
199 overall correlation between protein abundance and RNA expression across all seasons for gene in
200 both data sets (Supplemental Fig. S6, $R^2 = 0.14$). Analyzing differential abundance of proteins, we
201 found 124 proteins significantly changed ($p_{\text{adj}} < 0.05$) between summer juveniles and winter
202 juveniles (78 increased and 46 decreased in winter) (Fig. 3A). Thirty-four of these proteins
203 overlapped with differentially expressed genes, all but one with matching mRNA and protein
204 direction.

205

206 Ranked set enrichment for proteomics identified five enriched pathways ($p_{\text{adj}} < 0.05$), four of
207 which overlapped the RNA pathway enrichment (oxidative phosphorylation, Parkinson's disease,
208 Alzheimer's disease, Huntington's disease). Oxidative phosphorylation was the most enriched

209 pathway in both mRNA and protein expression and included 17 overlapping genes/proteins, 11 of
210 which were found to be significant in at least one of the data sets (*ATP5MG*, *NDUFB4*, *PPAI*,
211 *SDHB*, *NDUFV3*, *NDUFA6*, *NDUFB8*, *NDUFS3*, *ATP5PO*, *NDUFC2*, *NDUFS6*; all in the
212 same direction). Proteomic analysis did not reveal upregulation in the glycolysis/gluconeogenesis
213 ($p_{\text{adj}}=1.00$, $\text{NES}=0.66$) pathway, though all but one overlapping gene also increased in abundance
214 in proteomics, including three aldehyde dehydrogenase genes (*ALDH3A2*, $p_{\text{adj}}<0.01$, $\text{LFC}=0.64$;
215 *ALDH1B1*, $p_{\text{adj}}<0.01$, $\text{LFC}=0.81$; *ALDH9A1*, $p_{\text{adj}}=0.47$, $\text{LFC}=0.35$) (Fig. 4B). Similarly,
216 proteomic set enrichment analysis did not validate fatty acid metabolism enrichment ($p_{\text{adj}}=0.91$,
217 $\text{NES}=1.00$), but there was overlap (11 of 18 genes), including genes that encode proteins that
218 transport (*ACADM*, $p_{\text{adj}}=0.17$, $\text{LFC}=0.40$; *ACADVL*, $p_{\text{adj}}=0.26$, $\text{LFC}=0.35$) and breakdown of long
219 fatty acid chains (*ACOX1*, $p_{\text{adj}}<0.001$, $\text{LFC}=0.81$).

220

221 ***Comparison to hibernation reveals distinct gene expression signatures***

222 To assess whether Dehnel's phenomenon shares regulatory features with hibernation, we
223 compared differentially expressed genes in winter shrew livers to those identified in hibernating
224 *Mesocricetus auratus* (Syrian hamsters). Overlap between the two datasets was limited
225 (Supplemental Table S6): only nine genes were significantly upregulated in both species, while
226 22 were significantly downregulated in both ($\text{FDR}/p_{\text{adj}}<0.05$) (Supplemental Fig. S7). An
227 additional 19 genes overlapped but in opposite directions. Two overlapping genes (*ALDH1B1* and
228 *GPI*) are components of the glycolysis and gluconeogenesis pathway, as well as *ETNPPL*, a
229 fasting induced gene.

230

231 Pathway enrichment corroborates gene expression discordance between the two wintering
232 strategies. Only four pathways were significantly enriched in hibernating *M. auratus*
233 (Supplemental Data S7), and none overlapped with those enriched in wintering shrews. Those

234 included: proximal tubule bicarbonate reclamation ($p_{\text{adj}} < 0.05$, NES=2.01), circadian rhythm
235 ($p_{\text{adj}} < 0.05$, NES=1.92), mapk signaling ($p_{\text{adj}} < 0.05$, NES=1.71), and terpenoid backbone
236 biosynthesis ($p_{\text{adj}} < 0.01$, NES=-2.14). Although oxidative phosphorylation showed some signal of
237 upregulation in *M. auratus* (NES=1.58), it was not statistically significant ($p_{\text{adj}} = 0.15$).

238

239 ***Spring regrowth exhibits weaker transcriptomic and proteomic signals***

240 Comparisons between winter juveniles and spring adults (growth) showed extensive change in
241 gene expression coincident with metabolic change, but correlation with proteomics was weak
242 (Fig. 3B). Of 2,462 significantly differentially expressed genes, 1,130 were upregulated and the
243 rest downregulated in spring adults (Fig. 3B). Yet, differential mRNA expression only
244 significantly enriched two pathways, including the downregulation of cell cycle ($p_{\text{adj}} < 0.05$,
245 NES=-1.77) and proteasome ($p_{\text{adj}} < 0.05$, NES=-1.91) pathways (Supplemental Data S8).

246 Comparing protein abundance between winter juveniles and spring adults (growth), 183 proteins
247 showed significant change (42 increased and 141 decreased) (Fig. 3B) (Supplemental Data S9).
248 While 41 of these overlapped with significant differentially expressed genes, nearly a quarter of
249 them (10) were in the opposite direction. This is unsurprising, as the model between protein LFC
250 and mRNA LFC explains little variation ($R^2 = 0.02$, $F = 22.73$, $df = 1374$, $p < 0.001$) (Fig. 3B).

251 Ranked protein enrichment corroborated minimal correlation, as none of the 6 significant
252 pathways: starch and sucrose metabolism ($p_{\text{adj}} < 0.01$, NES=2.33), TCA cycle ($p_{\text{adj}} < 0.01$,
253 NES=2.28), cysteine and methionine metabolism ($p_{\text{adj}} < 0.05$, NES=2.13), valine, leucine, and
254 isoleucine degradation ($p_{\text{adj}} < 0.05$, NES=1.92), spliceosome ($p_{\text{adj}} < 0.05$, NES=-1.71), and cell
255 adhesion molecules ($p_{\text{adj}} < 0.05$, NES=-1.75), overlapped with mRNA gene set analyses. There
256 were, however, individual genes validated in change of direction with proteomic data found in
257 upregulated processes in winter juveniles that decreased in spring adults (LFC<0): oxidative

258 phosphorylation (*NDUFB4*, *PPAI*), gluconeogenesis (*ALDH3A2*, *PGK1*, *ALDH1B1*), and fatty
259 acid metabolism (*ACOX1*).

260

261 *Network analysis identifies FOXO signaling pathways regulating size plasticity*

262 Differential expression analyses focused on genes of high effect between two size extremes, but
263 large modules comprising genes of *small* effect could also play pivotal roles in regulating
264 metabolic changes across all seasons. We characterized interactions in expression among genes
265 and identified modules of coexpressed liver genes correlated with body size using weighted gene
266 co-expression network analysis (WGCNA) (Supplemental Data S10). We identified 37 modules
267 (Fig. 2), 11 of which were significantly associated with body size ($p < 0.05$). Among these, the
268 “grey60” module is a small gene network most positively correlated with larger body size ($n=352$
269 genes, $p < 0.001$, $r=0.85$, $df=21$) and the “blue” module is a large network positively correlated
270 with small body size ($n=3,224$ gene, $p < 0.001$, $r=-0.65$, $df=21$). However, the “red” module was
271 significant ($n=3,224$ gene, $p < 0.05$, $r=-0.41$, $df=21$) and had the highest proportion (0.414) of
272 genes that overlapped with Cluster 4 genes, that were upregulated during autumn and winter.
273 Although no KEGG pathways were significant after multiple test correction when testing for gene
274 set enrichment from the “grey60” module significant, metabolic pathways was highly significant
275 ($p < 0.01$). The “blue” module enriched ten KEGG pathways, including the proteasome ($p_{adj} < 0.01$,
276 nucleocytoplasmic transport ($p_{adj} < 0.01$, and autophagy in animals ($p_{adj} < 0.01$). Thirty-four KEGG
277 pathways from the “red” module significant genes were significant after multiple test correction
278 ($p_{adj} < 0.05$). These pathways included FOXO signaling ($p_{adj} < 0.01$), as well as pathways upstream
279 (MAPK signaling, $p_{adj} < 0.05$) and downstream (insulin resistance, $p_{adj} < 0.01$; longevity regulating
280 pathways, $p_{adj} < 0.05$) of this pathway (Supplemental Table S7).

281

282 **Discussion**

283 Eurasian common shrews, *Sorex araneus*, require constant food intake to sustain their
284 extraordinarily high metabolic rates throughout the year (Genoud et al. 2018). Maintaining their
285 energetic budget is particularly difficult in winter, as temperatures drop, along with available
286 food. Within a German shrew population, we found clear signs of a seasonal size plasticity
287 known as Dehnel's phenomenon (Dehnel 1949; Lázaro et al. 2018; Pucek 1965b) (Fig. 1A).
288 These shrews shrink in autumn through winter, with recovery in the ensuing spring. Using this
289 population with confirmed Dehnel's phenomenon, we identify seasonal changes to metabolism
290 and underlying regulatory processes.

291

292 We hypothesized that shrews rely on fat utilization to maintain metabolic homeostasis in winter,
293 as do hibernators, but unlike them, shrews rapidly turn over fat during shrinkage (Keicher et al.
294 2017). Both hibernators and winter shrews may experience similar depleted energy reserves, as
295 suggested by the shared upregulation of *ETNPPL*, a gene typically induced by fasting in mice to
296 regulate lipid homeostasis (White et al. 2021). Despite this common signal of energetic stress,
297 transcriptomic analyses of winter juvenile shrews revealed upregulation of key lipid metabolism
298 genes, including those involved in promoting fatty acid oxidation: acyl-CoA dehydrogenase
299 medium chain (*ACADM*), acyl-CoA dehydrogenase very long chain (*ACADVL*), and acyl-CoA
300 oxidase 1 (*ACOX1*) (Fig. 4B). Analysis of gene and protein expression within this pathway
301 (Supplemental Fig. S5) supports activation of fatty acid oxidation (Fig. 4A), but we cannot fully
302 rule out potential inhibitory effects without functional validations. For example, *ACOX1* encodes
303 the rate-limiting enzyme for oxidizing very long chain fatty acids and is critical for inter-organ
304 metabolic communication. Liver-specific knockouts of *ACOX1* in mice increase adipose tissue
305 browning and circulating levels of polyunsaturated omega-3 fatty acids (Lu et al. 2024).

306

307 Consistent with the role of *ACOX1* in lipid metabolism, in shrunken winter juvenile shrews we
308 observe an increase in *ACOX1* expression paired with a decrease in circulating levels of
309 polyunsaturated fatty acids (DHA and AA) (Fig. 1B/C). This contrasts with hibernators:
310 circulating DHA and AA rise significantly in wintering bears and hibernating arctic ground
311 squirrels (Chazarin et al. 2019; Elaine Epperson et al. 2011; Drew et al. 2001; Rice et al. 2021).
312 Regulatory similarities and metabolomic differences indicate hibernation and Dehnel's wintering
313 strategies rely upon lipid metabolism in the liver. While hibernators conserve fat reserves over
314 winter, shrews exhibit rapid fat turnover (Keicher et al. 2017), decreasing levels of
315 polyunsaturated fatty acids as they maintain activity in winter.

316

317 Regulatory changes related to mitochondrial function further highlight differences in metabolic
318 processes between Dehnel's phenomenon and hibernation. The strongest signal in both RNA and
319 protein expression was the upregulation of oxidative phosphorylation pathways in winter
320 juveniles, indicating pathway activation (Fig. 4A). These include 21 genes encoding
321 mitochondrial complex I subunit proteins (NDUFs) and the succinate dehydrogenase gene,
322 *SDHB*. Hibernators monitor energy expenditure through circadian rhythm pathways
323 (Supplemental Fig. S3), and conserve energy in part through reduced liver mitochondrial
324 oxidation in response to cold temperature (Chaffee et al. 1961; Staples and Brown 2008),
325 decreasing SDH activity (Armstrong and Staples 2010; Gehrich and Aprille 1988). This, in turn,
326 impairs cellular respiration as they lower body temperature and metabolic rate. In contrast, winter
327 juvenile shrews show upregulated oxidative phosphorylation pathways compared to summer
328 juveniles. While Dehnel's phenomenon reduces resting metabolic rate in winter (Taylor et al.
329 2013), shrews remain active and neither reduce their body temperature nor upregulate circadian
330 rhythm pathways as hibernators do. Mitochondrial regulation in shrews is therefore opposite to
331 that of hibernators and may use known temperature-sensitive oxidative phosphorylation pathways

332 to improve mitochondrial efficiency, enhance metabolic plasticity, or maintain internal
333 temperatures despite the reduction in metabolic rate and body size. This hypothesis can be tested
334 by examining mitochondrial oxygen consumption in the liver throughout Dehnel's phenomenon.
335
336 During autumn and winter, shrews appeared to meet their energetic needs by activating responses
337 similar to those triggered by starvation. When blood sugar is low, mammals promote
338 gluconeogenesis, a process in which the liver produces free glucose from non-carbohydrate
339 substrates to avoid cellular starvation (Rui 2014). This process has previously been linked to
340 seasonal size change in shrews (Hyvärinen 1984). Glucose-6-phosphatase (G6P) enzyme levels
341 peak during autumn and decline through spring, suggesting gluconeogenesis is highest in autumn
342 and early winter when snow is too scarce to offer insulation, increasing demand for glucose to
343 prevent starvation. We discovered an upregulation of gluconeogenesis pathways in winter
344 juveniles (Fig. 4), including the overexpression of aldehyde dehydrogenases (*ALDH1B1* and
345 *ALDH3A2*) and *G6PC1*. *G6PC1* encodes one of three subunits of G6PC, a key gluconeogenesis
346 enzyme in the final step of gluconeogenesis, which catalyzes the formation of D-glucose that can
347 then be released into the blood. We propose the upregulation of this gene, along with others in the
348 pathway, modulates the previously observed increase in gluconeogenesis (Hyvärinen 1984).
349 Alongside elevated lipid metabolism and oxidative phosphorylation, these findings indicate
350 shrews maximize all available energy resources during winter (Fig. 4).
351
352 Large changes in mRNA and proteins only weakly supported one another when comparing winter
353 juveniles to spring adults (Fig. 3B), but changes in gene networks across all seasons parallel
354 regrowth (Fig. 2). We identified a large network negatively correlated with body size and
355 enriched with genes involved in FOXO and insulin signaling. Central to this network is the
356 forkhead box transcription factor 1 (*FOXO1*), upregulated during shrinkage and downregulated

357 during growth. In mice, FOXO1 stimulates gluconeogenesis that promotes hepatic glucose
358 production and release (Matsumoto et al. 2007; Xiong et al. 2013; Zhang et al. 2006), which can
359 subsequently impede processes including lipid metabolism in response to fasting glucose levels
360 (Zhang et al. 2006; Tikhanovich et al. 2013; Xiong et al. 2013; Yang et al. 2021). In shrinking
361 and regrowing shrews, FOXO signaling may thus regulate organismal energy homeostasis and
362 size by simultaneously regulating both glucose and lipid use to meet changing energy demands.

363

364 Increased FOXO signaling, however, may incur costs to shrew longevity. In model organisms
365 such as *C. elegans*, *Drosophila*, mice and humans, FOXO1 overexpression can reduce size and
366 extend lifespan, while inhibition leads to aging and senescence (Gami and Wolkow 2006;
367 Hwangbo et al. 2004; Katic and Kahn 2005; Satoh et al. 2013). Compared to other mammals, *S.*
368 *araneus* evolved Dehnel's phenomenon, a rare size plasticity (Lázaro et al. 2018; Pucek 1965b;
369 Dehnel 1949), as well as disproportionately high metabolic rate (Taylor 1998) and short lifespan
370 (Healy et al. 2014). FOXO1 cycling could explain this unique combination of traits. Should
371 findings from model organisms apply in the shrew, FOXO1-dependent glucose utilization
372 regulates shrinking, reducing mortality during harsh winters but undermines shrew longevity
373 when reversed in spring as a terminal investment for growth and reproduction. Genes within this
374 network are therefore key candidates for exploring both the regulatory mechanisms of size
375 change in Dehnel's phenomenon and links between metabolic change and lifespan in mammals.

376

377 Our study has limitations that should temper interpretation of individual genes and proposed
378 functions. Both small sample sizes within seasons and the small effect size of spring regrowth
379 reduce statistical power and limit the resolution of gene-level inference in wild species (Todd et
380 al. 2016). While exploring pathway-level analyses can mitigate these constraints, animal- or cell-
381 based functional validations will be essential to test our hypotheses. For example, CRISPR

382 knockouts could clarify the roles of genes like *SDHB* and *FOXO1* in regulating mitochondrial
383 efficiency or blood glucose levels across seasons (Fig. 5). As several proposed mechanisms likely
384 involve inter-organ signaling, future studies should examine other tissues, including adipose
385 tissue, which mediates lipid turnover, and the brain, which undergoes extraordinary plasticity in
386 Dehnel's phenomenon.

387

388 Our work provides a framework to examine how seasonal metabolic remodeling distinct from
389 hibernation regulates body size and life span. We propose that shrews undergoing Dehnel's
390 phenomenon regulate gene expression to deplete fat stores, increase gluconeogenesis, and alter
391 oxidative phosphorylation in ways that seem coordinated by FOXO signaling (Fig. 5). These
392 pathways are well-known regulators of aging and energy balance in model organisms, and may
393 represent a conserved regulatory axis linking metabolism, size, and lifespan across mammals. By
394 uncovering molecular covariates of this rare wintering strategy, our findings open new directions
395 for studying natural models of regeneration, and its links to metabolic plasticity and longevity.

396

397 **Material and Methods**

398 *Sample Collection*

399 Eurasian common shrews were trapped (protocols authorized by Regierungspräsidium Freiburg,
400 Baden-Württemberg 35-9185.81/G-19/131) using insulated wooden traps in Radolfzell, Germany
401 (47.9684 N, 8.9761 E), at five different stages of development: large summer juveniles (n=5),
402 shrinking autumn juveniles (n=4), small winter juveniles (n=5), regrowing spring adults (n=5),
403 and regrown summer adults (n=5). Shrews were aged and sexed based on tooth wear, fur
404 appearance, and gonad development prior to euthanasia. Fewer females than males were sampled
405 in juvenile stages (n=6 females). At that age, shrews are prepubescent, not sexually dimorphic,
406 and a previous study (Lázaro et al. 2018) found only minor sex dimorphism in brain region size

407 change. Although female under sampling is unlikely to influence gene expression, sex was used
408 as a covariate in subsequent models, accounting for this sampling skew.

409

410 Blood was collected prior to perfusion through the heart, let stand for 15 minutes, spun down at
411 1200 rpm, the serum pipetted off and then stored at -80°C. Shrews were perfused under
412 anesthesia via the vascular system with PAXgene Tissue Fixative. Livers were removed and
413 weighed to confirm the occurrence of Dehnel's phenomenon, split in half for paired
414 transcriptomic and proteomic analyses, and then placed immediately into PAXgene Tissue
415 Stabilizer. All samples were placed in stabilizer (2-24 hours after extraction) and then stored in
416 liquid nitrogen. Body and liver weight were tested for significant change in mass using a *t*-test
417 between seasons.

418

419 ***Metabolomics***

420 Metabolite analysis was carried out by MS-Omics using a Thermo Scientific Vanquish LC
421 (UPLC) coupled to Thermo Q Exactive HF MS. Identification of compounds were performed at
422 four levels; Level 1: identification by retention times (compared against in-house authentic
423 standards), accurate mass (with an accepted deviation of 3 ppm), and MS/MS spectra, Level 2a:
424 identification by retention times (compared against in-house authentic standards), accurate mass
425 (with an accepted deviation of 3 ppm). Level 2b: identification by accurate mass (with an
426 accepted deviation of 3ppm), and MS/MS spectra. MetaboAnalyst was used to test for changes in
427 concentration between seasons (Pang et al. 2021). Concentrations for each sample were
428 normalized by the average concentration of summer adult samples, log transformed and auto
429 scaled (Supplemental Fig. S1A). A partial least squares discriminant analysis was used to explore
430 if classification of metabolites into clusters aligned with seasonality (Supplemental Fig. S1B). A
431 one-way ANOVA was used to test for any significant seasonal difference in metabolite

432 concentration, with p-values corrected with a false discovery rate of 0.05 (Supplemental Fig.
433 SIC). Within each significant metabolite, *t*-tests were used to identify pairwise differences in
434 mean between each season. Samples were hierarchically clustered using significant genes and
435 visualized using a heatmap (Fig. 1).

436

437 *RNA Sequencing*

438 RNA was extracted with a modified Qiagen Micro RNAeasy protocol for small amounts of
439 mammalian tissue (Yohe et al. 2020). RNA was sent to Genewiz for quality control, library
440 preparation, and sequencing. RNA quantity was measured with a NanoDrop spectrophotometer
441 and quality of RNA assessed with RNA ScreenTape. Libraries were prepared with standard
442 polyA selection and sequenced as 150bp pair-end reads (Illumina, target of 15-25 million reads
443 per sample).

444

445 *Differential Gene Expression Analysis*

446 Tests for differential gene expression were conducted to identify genes whose liver expression
447 changes during Dehnel's phenomenon. We trimmed adapters and filtered reads using fastp (Chen
448 et al. 2018) and removed samples with extreme read counts (~10-fold). Gene counts were
449 quantified by pseudo aligning to the 24,205 protein coding genes of the *S. araneus* genome
450 (mSorAra2; GCF_027595985.1) using kallisto (Bray et al. 2016). Counts were normalized for
451 each tissue using DESeq2 median of ratios (Love et al. 2014) in R (R Core Team 2022).

452

453 Exploratory analyses included a principal component analysis to assess global gene expression
454 patterns across seasons. To identify genes associated with seasonal stage, we applied a likelihood
455 ratio test (LRT) in DESeq2 (Love et al. 2014), comparing a full model that included sex and
456 seasonal stage (~sex+season) to a reduced model with only an intercept (~1). Genes with an

457 adjusted p-value < 0.01 were considered significantly associated with seasonal stage. Expression
458 profiles of these significant genes were then clustered to explore temporal dynamics using
459 DEGREport (v1.44) (Pantano 2025). As these genes had already been filtered for statistical
460 significance, and lacked a continuous ranking metric such as log fold change, we performed an
461 unranked Gene Ontology (GO) enrichment of KEGG pathways using DAVID Gene Functional
462 Classification Tool (Huang et al. 2009). We chose KEGG over other GO sets, as KEGG's
463 orthology mapping is easier to use for a non-model species such as *S. araneus*.

464

465 Next, summer juveniles and winter juveniles were compared to infer regulatory processes
466 associated with shrinkage, while winter juveniles were tested against spring adults to explore
467 processes linked to regrowth. Normalized counts for each gene were modeled as a function of sex
468 and season with a negative binomial generalized linear model in DESeq2, then we used a Wald
469 test to examine the statistical association between the log-fold change and the season parameter,
470 with p-values corrected using the Benjamini and Hochberg procedure (Benjamini and Hochberg
471 1995). We then identified significantly enriched pathways with differentially expressed genes
472 using a ranked gene set enrichment of KEGG pathways using FGSEA (Korotkevich et al. 2021).
473 We chose a ranked gene set enrichment as it avoids an arbitrary threshold of significance,
474 considering the entire gene list of both upregulated and downregulated genes.

475

476 To compare gene expression during Dehnel's phenomenon to patterns observed in hibernation,
477 we obtained liver transcriptomic results from hibernating *Mesocricetus auratus* (Syrian hamsters,
478 NCBI GEO accession number GSE199814) (Coussement et al. 2023). As small mammals with
479 high metabolic rates, Syrian hamsters provide a physiologically comparable model to common
480 shrews than large-bodied hibernators such as bears. We performed a ranked gene set enrichment
481 analysis using the approach described above. To identify overlap, we compared significantly

482 enriched pathways as well as individual genes ($p_{adj}<0.05$) that were differentially expressed in
483 both data sets.

484

485 ***Weighted Gene Co-expression Network Analysis***

486 We used the WGCNA package (Langfelder and Horvath 2008) package to create co-expression
487 networks for the liver and determined if these correlations between genes were significantly
488 correlated with body size. We calculated the Pearson's correlation for expression between each
489 gene pair, which was then transformed to an adjacency matrix using a soft-threshold power
490 adjacency function described in Langfelder and Horvath (Langfelder and Horvath 2008). The
491 power function reduced the spurious connectivity between genes from noise by increasing
492 sensitivity, and its appropriate scale was determined by maximizing the scale-free topology
493 criterion (maximizing model fit while saturating mean connectivity). The resulting adjacency
494 matrix was then used to calculate a topological overlap matrix (dissimilarity matrix), in which
495 dissimilarity distances grouped genes into modules using fuzzy, cmeans hierarchical clustering.
496 We removed any module with fewer than 25 genes, and merged gene modules that were found to
497 have similar eigengene values. Then, eigengene significance between the correlation of body size
498 to each module's eigengene value was calculated. Cytoscape (Shannon et al. 2003) was used to
499 visualize significant networks and calculate network statistics such as node (gene) connectivity.
500 Enrichments for each module were analyzed using DAVID to test for GO enrichment (Huang et
501 al. 2009), and module genes were compared to those identified using the LRT.

502

503 ***Proteomics***

504 Liver tissue from *Sorex araneus* was isolated and protein homogenates were prepared by
505 transferring the liver tissue to a dissection buffer containing 10% sucrose (VWR), imidazole
506 (Merck Millipore), EDTA (Sigma-Aldrich), Pefabloc (Sigma-Aldrich) and leupeptin (VWR). The

507 mixture was homogenized (T10 basic ULTRA-TURAX homogenizer IKA®) for 20 sec; then,
508 samples were centrifuged at 1000 g for 15 min. Supernatants were stored at -20°C. Proteomic
509 sample preparation was performed using the PreOmics, Cat. No.: 00027 iST 96x kit. The samples
510 were vacuum centrifuged overnight, and the dry peptide product was stored at -80°C until
511 analysis.

512

513 Peptides were resuspended in a solution containing 2% acetonitrile (ACN), 0.1% formic acid
514 (FA) and 0.1% TFA, and then, peptides were briefly sonicated. Five micrograms of total peptide
515 material were analyzed per liquid chromatography–mass spectrometry analysis. Samples were
516 analyzed using a UPLC-nanoESI MS/MS setup with a NanoRSLC system (Dionex, Sunnyvale,
517 CA, USA). The system was coupled online with an emitter for nanospray ionization (New
518 Objective PicoTip 360-20-10) to a Q Exactive HF mass spectrometer (Thermo Scientific,
519 Waltham, USA). The peptide material was loaded onto a 2-cm trapping reversed-phase Acclaim
520 PepMap RSLC C18 column (Dionex) and separated using an analytical 75-cm reversed-phase
521 Acclaim PepMap RSLC C18 column (Dionex). Both columns were kept at 60°C. The sample was
522 eluted with a gradient of 90% solvent A (0.1% FA, 0.1% TFA) and 10% solvent B (0.1% FA,
523 0.1% TFA in ACN), which was increased to 7% solvent B on a 1-min ramp gradient at a constant
524 flow rate of 300 nL/min. Subsequently, the gradient was raised to 30% solvent B on a 45-min
525 ramp gradient. The mass spectrometer was operated in positive mode, selecting up to 20
526 precursor ions with a mass window of m/z 1.6 based on highest intensity for higher-energy
527 collisional dissociation (HCD) fragmenting at a normalized collision energy of 27. Selected
528 precursors were dynamically excluded for fragmentation for 30 s.

529

530 A label-free relative quantitation analysis was performed using MaxQuant 1.5.7.4 software
531 (Tyanova et al. 2016a). Raw files were searched against the *S. araneus* genome assembly

532 (GCF_027595985.1_mSorAra2.pri_genomic.gtf). All standard settings were employed with
533 carbamidomethylation (C) as a static peptide modification and deamidation (NQ), oxidation (M),
534 formylation (N-terminal and K), and protein acetylation (N-terminal) as variable modifications.
535 The output contained a list of proteins identified <1% false discovery rate, and their abundances
536 were further filtered and processed using the Perseus v1.5.6.0 platform (Tyanova et al. 2016b).
537 All reverse hits that identified proteins were removed from further analysis, and the data were
538 log₂-transformed to approximate a normal distribution. Two or more unique peptides were
539 required for protein quantitation. Additionally, a non-zero quantitation value in at least 70% of
540 the samples in one of the groups was required from quantifiable proteins. The mass spectrometry
541 proteomics data have been deposited to the ProteomeXchange Consortium
542 (<http://proteomecentral.proteomexchange.org>) via the PRIDE partner repository (Perez-Riverol et
543 al. 2025) with the dataset identifier PXD068559 and doi: 10.6019/PXD068559.

544

545 After preprocessing, we inferred potential functional changes associated with differences in
546 protein abundances and analyzed correlations with transcriptomic data. First, the label-free
547 quantitation matrix was restricted to summer-juvenile and winter-juvenile samples. Differential
548 protein abundance was evaluated in Perseus (v1.5.6.0) with its permutation-based two-sided
549 Student's *t*-test (250 randomizations; no group preservation). We corrected for multiple testing
550 via the Benjamini–Hochberg procedure with a false-discovery rate of 5%. A S_0 constant of 0.1
551 was added to stabilize variance in the SAM-like statistic. Significantly differentially abundant
552 proteins ($p_{\text{adj}} < 0.05$) were displayed in a volcano plot. We then identified significantly enriched
553 pathways of protein using a ranked gene set enrichment of KEGG pathways using FGSEA
554 (Korotkevich et al. 2021).

555

556 To investigate the relationship between seasonal changes in protein abundance and RNA
557 abundance, we also quantified Pearson's correlation coefficients between log-transformed protein
558 abundance and normalized RNA expression across all samples. We also performed two linear
559 regression analyses to observe protein and RNA concordance. First, log-transformed RNA counts
560 was modeled as a function of the corresponding protein abundance using the `lm` function in R.
561 Second, differential protein abundance was modeled as a function of the corresponding gene
562 expression log-fold change.

563

564 **Data Access**

565 The raw RNA sequencing data generated in this study have been submitted to the NCBI
566 BioProject data base under accession number [PRJNA941271](https://www.ncbi.nlm.nih.gov/bioproject/PRJNA941271). The mass spectrometry proteomics
567 data generated in this study have been submitted to the ProteomeXchange Consortium via the
568 PRIDE partner repository with the dataset identifier PXD068559 and doi: 10.6019/PXD068559.
569 The raw metabolomics data generated in this study have been submitted to Metabolomics
570 Workbench (Sud et al. 2016) with a project identifier PR002691, Study ID ST004264, and doi:
571 [10.21228/M8T837](https://doi.org/10.21228/M8T837). Processed data and results can be found in the Supplementary Materials and
572 are publicly available on Dryad <https://doi.org/10.5061/dryad.pc866t1w3>. Reproducible code to
573 complete these analyses can be found in the Supplemental Code and on GitHub:
574 https://github.com/wrthomas315/Dehnels_Seasonal_RNAseq2/tree/main/data.

575

576 **Competing Interests**

577 The authors declare that they have no conflict of interest.

578

579 **Acknowledgments**

580 We thank Joshua Rest, Krishna Veeramah, and Tanya Lama who have provided helpful feedback
581 on initial results and previous versions of the manuscript. We thank Michal Oklinski for help with
582 initial dissections. We also thank NIH funding (U2C-DK119886 and OT2-OD030544) to
583 Metabolomics Workbench for raw data submission.

584

585 **Author Contributions and Funding Disclosure**

586 LMD, DD, APC, and JN conceived and funded project. CB, MM, and DD collected, measured,
587 and sampled shrews. WRT designed and conducted genomic analyses. WRT, JHJ, JN, and APC
588 analyzed metabolite concentrations. TB performed the LC/MS/MS and correlated with shrew
589 database. WRT and YZ analyzed proteomic results. WRT visualized data and wrote initial
590 draft. LMD, DD, JN, DC, and APC contributed to review and editing of draft. All authors
591 contributed to data interpretation. WRT and research were supported by the Human Frontiers in
592 Science Program Award (RGP0013/2019) to DD, LMD, and JN, and by the Stony Brook
593 University Presidential Innovation and Excellence Fund to LMD.

594

595 **References**

- 596 Armstrong C, Staples JF. 2010. The role of succinate dehydrogenase and oxaloacetate in
597 metabolic suppression during hibernation and arousal. *J Comp Physiol B Biochem Syst*
598 *Environ Physiol* **180**: 775–783.
- 599 Auteri GG. 2022. A conceptual framework to integrate cold-survival strategies: Torpor, resistance
600 and seasonal migration. *Biol Lett* **18**: 1–6.
- 601 Benjamini Y, Hochberg Y. 1995. Controlling the False Discovery Rate : A Practical and Powerful
602 Approach to Multiple Testing. *J R Stat Soc* **57**: 289–300.
- 603 Boyer BB, Barnes BM. 1999. Molecular and metabolic aspects of mammalian hibernation.
604 *Bioscience* **49**: 713–724.
- 605 Bray NL, Pimentel H, Melsted P, Pachter L. 2016. Near-optimal probabilistic RNA-seq
606 quantification. *Nat Biotechnol* **34**: 525–527.
- 607 Chaffee RR, Hoch FL, Lyman CP. 1961. Mitochondrial oxidative enzymes and phosphorylations
608 in cold exposure and hibernation. *Am J Physiol* **201**: 29–32.
- 609 Chazarin B, Storey KB, Ziemianin A, Chanon S, Plumel M, Chery I, Durand C, Evans AL,
610 Arnemo JM, Zedrosser A, et al. 2019. Metabolic reprogramming involving glycolysis in the
611 hibernating brown bear skeletal muscle. *Front Zool* **16**: 1–21.
- 612 Chen S, Zhou Y, Chen Y, Gu J. 2018. Fastq: An ultra-fast all-in-one FASTQ preprocessor.
613 *Bioinformatics* **34**: i884–i890.
- 614 Churchfield S, Rychlik L, Taylor JRE. 2012. Food resources and foraging habits of the common
615 shrew, *Sorex araneus*: Does winter food shortage explain Dehnel’s phenomenon? *Oikos*
616 **121**: 1593–1602.
- 617 Coussemont L, Oosterhof MM, Guryev V, Reitsema VA, Bruintjes JJ, Goris M, Bouma HR, De
618 Meyer T, Rots MG, Henning RH. 2023. Liver transcriptomic and methylomic analyses
619 identify transcriptional mitogen-activated protein kinase regulation in facultative
620 hibernation of Syrian hamster. *Proc R Soc B Biol Sci* **290**.
- 621 Dehnel A. 1949. Studies of the genus *Sorex* L. *Ann Univ M Curie-Sklod* **4**: 17–104.
- 622 Drew KL, Rice ME, Kuhn TB, Smith MA. 2001. Neuroprotective adaptations in hibernation:
623 Therapeutic implications for ischemia-reperfusion, traumatic brain injury and
624 neurodegenerative diseases. *Free Radic Biol Med* **31**: 563–573.
- 625 Elaine Epperson L, Karimpour-Fard A, Hunter LE, Martin SL. 2011. Metabolic cycles in a
626 circannual hibernator. *Physiol Genomics* **43**: 799–807.
- 627 Faherty SL, Luis Villanueva-Cañas J, Klopfer PH, Albà MM, Yoder AD. 2016. Gene expression
628 profiling in the hibernating primate, *Cheirogaleus medius*. *Genome Biol Evol* **8**: 2413–2426.
- 629 Gami MS, Wolkow CA. 2006. Studies of *Caenorhabditis elegans* DAF-2/insulin signaling reveal
630 targets for pharmacological manipulation of lifespan. *Aging Cell* **5**: 31–37.
- 631 Gehnrich SC, Aprille JR. 1988. Hepatic gluconeogenesis and mitochondrial function during
632 hibernation. *Comp Biochem Physiol -- Part B Biochem* **91**: 11–16.
- 633 Genoud M, Isler K, Martin RD. 2018. Comparative analyses of basal rate of metabolism in
634 mammals : data selection does matter. *Biol Rev* **93**: 404–438.
- 635 Healy K, Guillerme T, Finlay S, Kane A, Kelly SBA, McClean D, Kelly DJ, Donohue I, Jackson
636 AL, Cooper N. 2014. Ecology and mode-of-life explain lifespan variation in birds and
637 mammals. *Proc R Soc B* **281**: 20140298.
- 638 Huang DW, Sherman BT, Lempicki RA. 2009. Systematic and integrative analysis of large gene
639 lists using DAVID bioinformatics resources. *Nat Protoc* **4**: 44–57.
- 640 Hwangbo DS, Garsham B, Tu MP, Palmer M, Tatar M. 2004. *Drosophila* dFOXO controls
641 lifespan and regulates insulin signalling in brain and fat body. *Nature* **429**: 562–566.
- 642 Hyvärinen H. 1984. Wintering strategy of voles and shrews in Finland. *Winter Ecol Small*

- 643 *Mamm* **10**: 139–148.
- 644 Katic M, Kahn CR. 2005. The role of insulin and IGF-1 signaling in longevity. *Cell Mol Life Sci*
645 **62**: 320–343.
- 646 Keicher L, O'Mara MT, Voigt CC, Dechmann DKN. 2017. Stable carbon isotopes in breath
647 reveal fast metabolic incorporation rates and seasonally variable but rapid fat turnover in the
648 common shrew (*Sorex araneus*). *J Exp Biol* **220**: 2834–2841.
- 649 Korotkevich G, Sukhov V, Budin N, Atryomov MN, Sergushichev A. 2021. Fast gene set
650 enrichment analysis. *bioRxiv*.
- 651 Langfelder P, Horvath S. 2008. WGCNA: An R package for weighted correlation network
652 analysis. *BMC Bioinformatics* **9**.
- 653 Lázaro J, Dechmann DKN. 2021. Dehnel's phenomenon. *Curr Biol* **31**: R463–R465.
- 654 Lázaro J, Hertel M, Muturi M, Dechmann DKN. 2019. Seasonal reversible size changes in the
655 braincase and mass of common shrews are flexibly modified by environmental conditions.
656 *Sci Rep* **9**: 1–10.
- 657 Lázaro J, Hertel M, Sherwood CC, Muturi M, Dechmann DKN. 2018. Profound seasonal changes
658 in brain size and architecture in the common shrew. *Brain Struct Funct* **223**: 2823–2840.
- 659 Love MI, Huber W, Anders S. 2014. Moderated estimation of fold change and dispersion for
660 RNA-seq data with DESeq2. *Genome Biol* **15**: 1–21.
- 661 Lu D, He A, Tan M, Mrad M, El Daibani A, Hu D, Liu X, Kleiboeker B, Che T, Hsu FF, et al.
662 2024. Liver ACOX1 regulates levels of circulating lipids that promote metabolic health
663 through adipose remodeling. *Nat Commun* **15**.
- 664 Matsumoto M, Pocai A, Rossetti L, DePinho RA, Accili D. 2007. Impaired Regulation of Hepatic
665 Glucose Production in Mice Lacking the Forkhead Transcription Factor Foxo1 in Liver.
666 *Cell Metab* **6**: 208–216.
- 667 Pang Z, Chong J, Zhou G, De Lima Morais DA, Chang L, Barrette M, Gauthier C, Jacques PÉ, Li
668 S, Xia J. 2021. MetaboAnalyst 5.0: Narrowing the gap between raw spectra and functional
669 insights. *Nucleic Acids Res* **49**: 388–396.
- 670 Pantano L. 2025. DEGREport: Report of DEG analysis.
- 671 Perez-Riverol Y, Bandla C, Kundu DJ, Kamatchinathan S, Bai J, Hewapathirana S, John NS,
672 Prakash A, Walzer M, Wang S, et al. 2025. The PRIDE database at 20 years: 2025 update.
673 *Nucleic Acids Res* **53**: D543–D553.
- 674 Pucek M. 1965a. Water contents and seasonal changes of the brain-weight in shrews. *Acta*
675 *Theriol (Warsz)* **10**: 353–367.
- 676 Pucek Z. 1965b. Seasonal and age changes in the weight of internal organs of shrews. *Acta*
677 *Theriol (Warsz)* **10**: 369–438.
- 678 R Core Team. 2022. R: A language and environment for statistical computing. R Foundation for
679 Statistical Computing.
- 680 Ray S, Li M, Koch SP, Mueller S, Boehm-Sturm P, Wang H, Brecht M, Naumann RK. 2020.
681 Seasonal plasticity in the adult somatosensory cortex. *Proc Natl Acad Sci U S A* **117**:
682 32136–32144.
- 683 Rice SA, Mikes M, Bibus D, Berdyshev E, Reisz JA, Gehrke S, Bronova I, D'Alessandro A,
684 Drew KL. 2021. Omega 3 fatty acids stimulate thermogenesis during torpor in the Arctic
685 Ground Squirrel. *Sci Rep* **11**: 1–14.
- 686 Rui L. 2014. Energy Metabolism in the Liver Liangyou Rui. *Physiol Behav* **176**: 139–148.
- 687 Satoh A, Brace CS, Rensing N, Cliften P, Wozniak DF, Herzog ED, Yamada KA, Imai SI. 2013.
688 Sirt1 extends life span and delays aging in mice through the regulation of Nk2 Homeobox 1
689 in the DMH and LH. *Cell Metab* **18**: 416–430.
- 690 Schaeffer PJ, O'Mara MT, Breiholz J, Keicher L, Lázaro J, Muturi M, Dechmann DKN. 2020.
691 Metabolic rate in common shrews is unaffected by temperature, leading to lower energetic

- 692 costs through seasonal size reduction. *R Soc Open Sci* **7**.
- 693 Shannon P, Markiel A, Ozier O, Nitin SB, Wang JT, Ramage D, Amin N, Schwikowski B, Ideker
694 T. 2003. Cytoscape: A Software Environment for Integrated Models. *Genome Res* **13**:
695 2498–2504.
- 696 Staples JF, Brown JCL. 2008. Mitochondrial metabolism in hibernation and daily torpor: A
697 review. *J Comp Physiol B Biochem Syst Environ Physiol* **178**: 811–827.
- 698 Sud M, Fahy E, Cotter D, Azam K, Vadivelu I, Burant C, Edison A, Fiehn O, Higashi R, Nair
699 KS, et al. 2016. Metabolomics Workbench: An international repository for metabolomics
700 data and metadata, metabolite standards, protocols, tutorials and training, and analysis tools.
701 *Nucleic Acids Res* **44**: D463–D470.
- 702 Taylor JRE. 1998. Evolution of Energetic Strategies in Shrews. In *Evolution of Shrews*, pp. 309–
703 346.
- 704 Taylor JRE, Rychlik L, Churchfield S. 2013. Winter reduction in body mass in a very small,
705 nonhibernating mammal: Consequences for heat loss and metabolic rates. *Physiol Biochem*
706 *Zool* **86**: 9–18.
- 707 Tikhanovich I, Cox J, Weinman SA. 2013. Forkhead box class O transcription factors in liver
708 function and disease. *J Gastroenterol Hepatol* **28**: 125–131.
- 709 Todd E V., Black MA, Gemmell NJ. 2016. The power and promise of RNA-seq in ecology and
710 evolution. *Mol Ecol* **25**: 1224–1241.
- 711 Tyanova S, Temu T, Cox J. 2016a. The MaxQuant computational platform for mass
712 spectrometry-based shotgun proteomics. *Nat Protoc* **11**: 2301–2319.
- 713 Tyanova S, Temu T, Sinitcyn P, Carlson A, Hein MY, Geiger T, Mann M, Cox J. 2016b. The
714 Perseus computational platform for comprehensive analysis of (prote)omics data. *Nat*
715 *Methods* **13**: 731–740.
- 716 Villanueva-Cañas JL, Faherty SL, Yoder AD, Albà MM. 2014. Comparative genomics of
717 mammalian hibernators using gene networks. *Integr Comp Biol* **54**: 452–462.
- 718 Weir K, Vega N, Busa VF, Sajdak B, Kallestad L, Merriman D, Palczewski K, Carroll J,
719 Blackshaw S. 2024. Identification of shared gene expression programs activated in multiple
720 modes of torpor across vertebrate clades. *Sci Rep* **14**: 24360.
- 721 White CJ, Ellis JM, Wolfgang MJ. 2021. The role of ethanolamine phosphate phospholyase in
722 regulation of astrocyte lipid homeostasis. *J Biol Chem* **297**: 100830.
- 723 Xiong X, Tao R, DePinho RA, Dong XC. 2013. Deletion of Hepatic FoxO1/3/4 Genes in Mice
724 Significantly Impacts on Glucose Metabolism through Downregulation of Gluconeogenesis
725 and Upregulation of Glycolysis. *PLoS One* **8**: 1–11.
- 726 Yang Z, Roth K, Agarwal M, Liu W, Petriello MC. 2021. The transcription factors CREBH,
727 PPARα, and FOXO1 as critical hepatic mediators of diet-induced metabolic dysregulation. *J*
728 *Nutr Biochem* **95**: 108633.
- 729 Yohe LR, Davies KTJ, Simmons NB, Sears KE, Dumont ER, Rossiter SJ, Dávalos LM. 2020.
730 Evaluating the performance of targeted sequence capture, RNA-Seq, and degenerate-primer
731 PCR cloning for sequencing the largest mammalian multigene family. *Mol Ecol Resour* **20**:
732 140–153.
- 733 Zhang W, Patil S, Chauhan B, Guo S, Powell DR, Le J, Klotsas A, Matika R, Xiao X, Franks R,
734 et al. 2006. FoxO1 regulates multiple metabolic pathways in the liver effects on
735 gluconeogenic, glycolytic, and lipogenic gene expression. *J Biol Chem* **281**: 10105–10117.
- 736
- 737

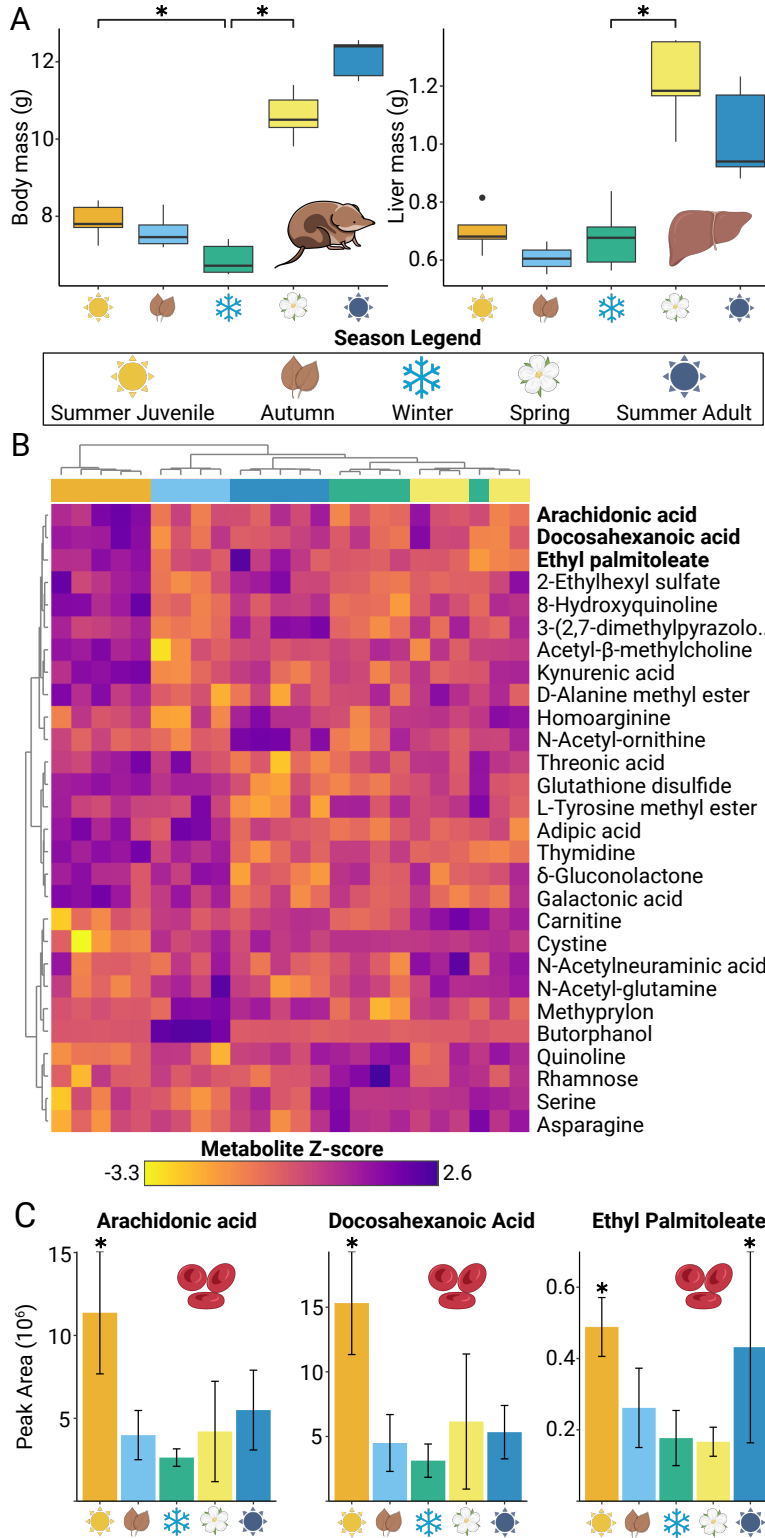
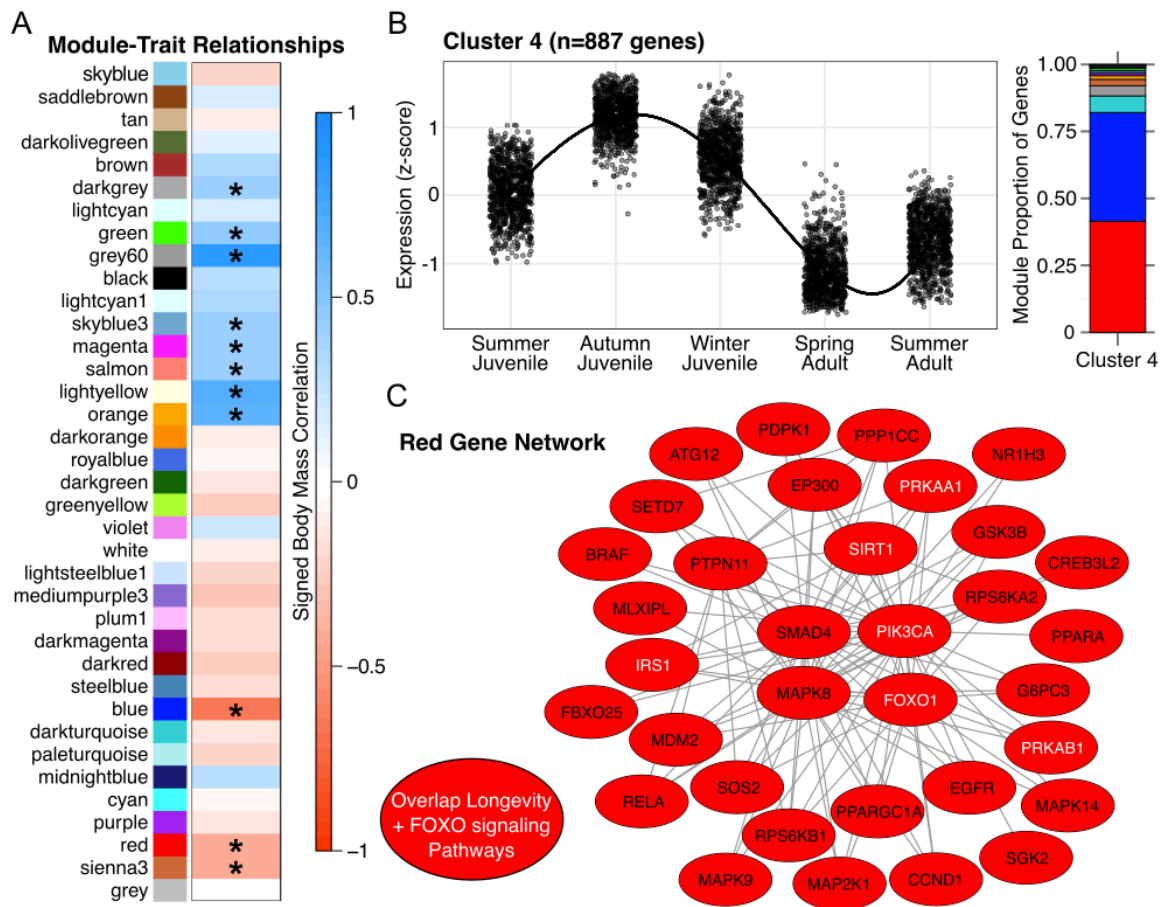


Figure 1. Confirming Dehnel's phenomenon and metabolic profiling of the blood metabolome. (A) Mass change of body and liver through a year of Dehnel's phenomenon. Both the body and the liver begin to decrease in mass as autumn juveniles, with body mass at a minimum as winter juveniles, proceeded by regrowth as spring adults. Asterisks represent significant size changes (adjusted $p < 0.05$). **(B)** Heatmap of 28 statistically significant differentially concentrated metabolites between stages of Dehnel's phenomenon. Hierarchical clustering using these significant metabolites groups each profile into each season. **(C)** Three of these metabolites were lipid metabolites (ethyl palmitoleate, docosahexanoic acid, arachidonic acid), with decreases in autumn, winter, and spring individuals.

768

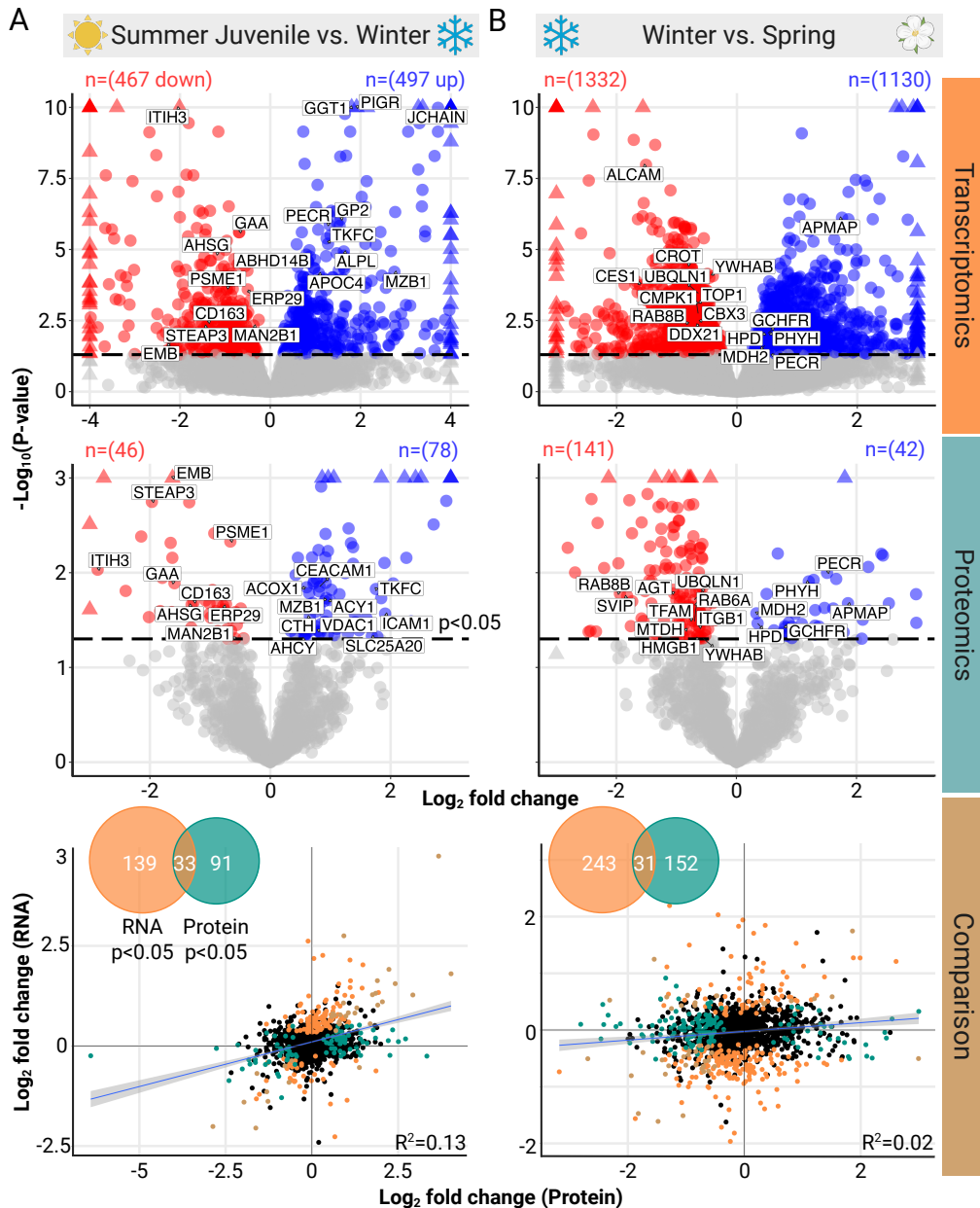


769

770

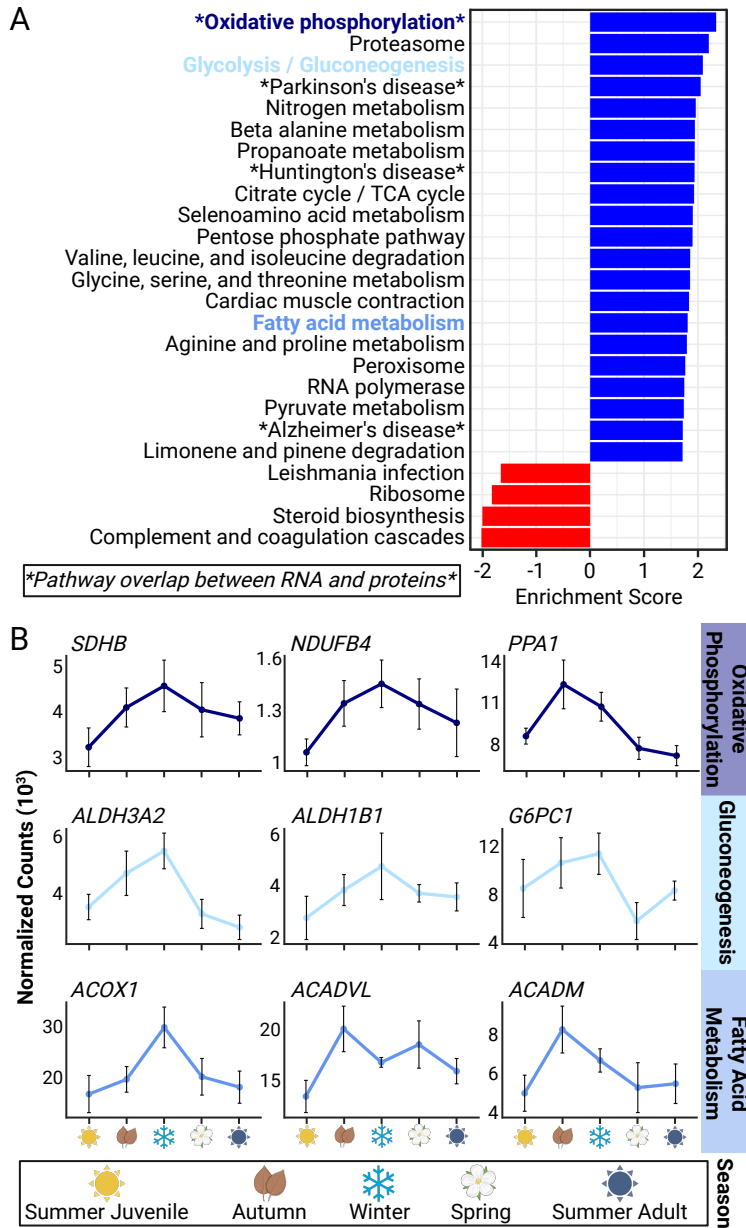
771 **Figure 2. Gene networks highly correlated with seasonal body size plasticity.** (A) Gene
 772 expression correlations form 37 modules. Eleven of these modules were significantly correlated
 773 with shrew body size. (B) Clustering of significant genes across seasons (LRT, $p_{adj} < 0.05$)
 774 revealed a cluster of genes (Cluster 4) with upregulation during shrinking seasons. The largest
 775 proportion of these genes overlapped with the red gene network. (C) Pathway enrichment of the
 776 large (n=3268 genes) “red” module highlighted functional associations to FOXO signaling and
 777 insulin resistance (plotted genes), which are associated with longevity regulating pathways.

778



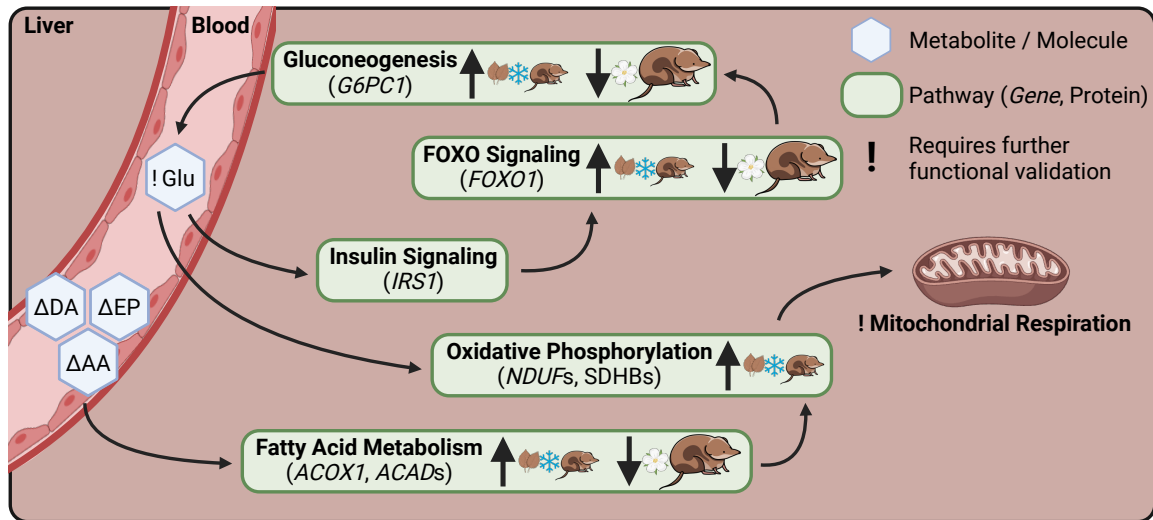
779

780 **Figure 3. Seasonal regulatory (transcriptomics and proteomics) change in the shrew liver.**
 781 **(A)** Volcano plots of significant ($p_{adj} < 0.05$) differentially expressed genes and proteins (colored)
 782 for summer vs. winter juvenile comparisons. Triangles represent lower p-values ($-\log(p) > 10$) or
 783 log fold changes ($abs(LFC) > 4$) beyond the limits of the graph. Correlation of log fold change and
 784 significant gene overlap between RNA and protein indicate high association between multi-omic
 785 comparisons ($R^2 = 0.13$). **(B)** While volcano plots of significant differentially expressed genes and
 786 proteins for winter juveniles vs. spring adult were identified, multi-omic correlation were low in
 787 comparison to the shrinking phase ($R^2 = 0.02$).



788
 789
 790
 791
 792
 793
 794

Figure 4. Seasonal changes in pathways associated with Dehnel's phenomenon (A) Pathway enrichment of summer vs winter juveniles between RNA (shown) and protein analyses, both with the largest enrichment of oxidative phosphorylation pathways. **(B)** Normalized gene counts in seasonally changing pathways of interest.



795
796
797
798
799
800
801
802
803
804

Figure 5. Summary of dynamic changes in shrew metabolism associated with seasonal size change, with proposed regulation of Dehnel’s cycle. Depleted lipid metabolites in the blood and increased RNA expression of genes involved in fatty acid metabolism indicate rapid fat turnover in winter juveniles. FOXO signaling regulates gluconeogenesis, also upregulated in winter juveniles, providing another energy source. Both FOXO signaling and fatty acid metabolism promote changes in oxidative phosphorylation, as was found in both transcriptomic and proteomic analyses, and have large effects on mitochondrial respiration in the liver.